Journal of Power Sources 234 (2013) 139–146

Contents lists available at SciVerse ScienceDirect

Journal of Power Sources

journal homepage: www.elsevier.com/locate/jpowsour

Influence of different anchoring groups in indoline dyes for dye-sensitized solar cells: Electron injection, impedance and charge recombination

Bo Liu [a,c,1], Wenqin Li [b,1], Bao Wang [a], Xiaoyan Li [a], Qingbin Liu [a,**], Yoshinori Naruta [c], Weihong Zhu [b,*]

[a] College of Chemistry and Material Science, Hebei Normal University, No. 20, East Road of Nan Er Huan, Shijiazhuang 050023, PR China
[b] Shanghai Key Laboratory of Functional Materials Chemistry, Key Laboratory for Advanced Materials, Institute of Fine Chemicals, East China University of Science & Technology, 130 Meilong Road, Shanghai 200237, PR China
[c] Institute for Materials Chemistry and Engineering and International Institute for Carbon-Neutral Energy Research (WPI-I^{2}CNER), Kyushu University, Fukuoka 812-8581, Japan

HIGHLIGHTS

- The influence of different anchoring groups on photovoltaic performances is focused.
- The photovoltaic efficiency of C-RA (0.57–0.90%) is much less than that of C-CA (8.49%).
- The low photo-excited electron injection efficiency in C-RA results in low J_{SC}.
- Both low charge density and fast recombination rate in C-RA lead to low V_{OC}.

GRAPHICAL ABSTRACT

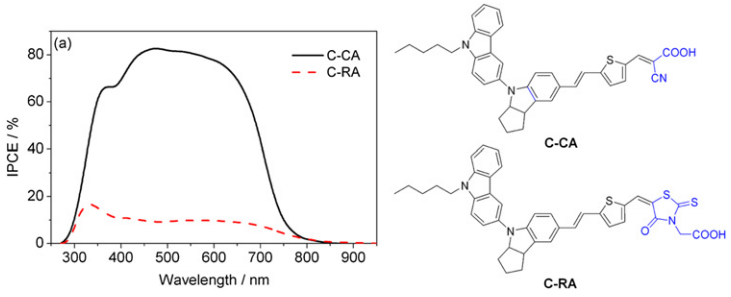

ARTICLE INFO

Article history:
Received 24 July 2012
Received in revised form
24 November 2012
Accepted 25 January 2013
Available online 7 February 2013

Keywords:
Solar cells
Indoline
Rhodanine
Acceptor
Charge recombination

ABSTRACT

For developing panchromatic dyes, we focus on the effect of rhodanine acceptor on photovoltaic performances in D-π-A indoline dye. Upon changing from cyanoacetic acid (dye C-CA) to rhodanine-3-acetic acid (dye C-RA) as acceptor and anchoring group, C-RA shows broader absorption band, which can overlap with the solar spectrum more preferably. However, the power conversion efficiency of DSSCs based on C-RA (0.57–0.90%) is one order of magnitude with respect to C-CA (8.49%). The distinct difference of IPCE values between C-CA and C-RA is predominately attributed to the different excited electron injection yield (Φ_{inj}). The relatively short excited electron lifetime and the isolation of LUMO orbital from anchoring group in C-RA result in the low photo-excited electron injection efficiency with low J_{SC}. Moreover, with respect to C-CA, the systematic SLIT and EIS studies demonstrate that C-RA possesses the relatively low injection charge density in the TiO_2 electrode and fast charge recombination rate, leading to a low V_{OC}. Our studies are highly helpful to the design of novel metal-free D-π-A organic sensitizers, especially for those using rhodanine-3-acetic acid as acceptor.

1. Introduction

Dye-sensitized solar cells (DSSCs) have attracted considerable attention due to their high performance and the potential of low-cost production [1–5]. As a critical component in DSSCs, metal-free organic sensitizers have been extensively explored in recent years due to their low material costs, ease of structural modification, high molar extinction coefficients, and environment-friendly characteristics [6–10]. Among them, indoline dyes have

* Corresponding author. Tel.: +86 21 6425 0772; fax: +86 21 6425 2758.
** Corresponding author.
E-mail addresses: qbinliu@yahoo.com (Q. Liu), whzhu@ecust.edu.cn (W. Zhu).
[1] These authors contributed equally to this work.

0378-7753/$ – see front matter © 2013 Elsevier B.V. All rights reserved.
http://dx.doi.org/10.1016/j.jpowsour.2013.01.152

become a kind of the most promising organic sensitizers [11,12]. However, their power conversion efficiencies (η) are still lower than those of classic ruthenium dyes [13–15]. One of the most important drawbacks is their relatively narrow absorption spectra in visible region, a stumbling block in the enhancement of short-circuit photocurrent density (J_{SC}) [16]. Accordingly, many efforts have focused on developing panchromatic photo-responsive indoline based sensitizers [17–22]. The first indoline dye, coded as D102, was synthesized by Horiuchi et al. in 2003 [11]. Its maximum peak (λ_{max}) was found at 491 nm in a mixture solution of *t*-butyl alcohol/acetonitrile, and the onset wavelength was at about 600 nm. To increase the light harvesting capability, an additional rhodanine unit was introduced into acceptor to develop dyes D149 and D205 [17,19]. Compared to D102, the λ_{max} and the onset wavelength of D149 were successfully red-shifted to 526 and 650 nm, respectively, resulting in a sharply increase in photovoltaic efficiency (η).

With our continuous interests in indoline sensitizers [23–29], we are also intrigued to expand the photo-responsive area to whole visible region, even to near-infrared region (NIR). More recently, we have introduced an additional carbazole unit into indoline segment (C-CA), resulting in a broad absorption spectrum covered from ultraviolet region to 763 nm [29]. However, its absorbance as well as IPCE values in NIR region is still low. Moreover, its absorbance in organic solvents is lower than 5% of maximum value in the region of longer than 690 nm, meaning that C-CA is not a practically panchromatic sensitizer.

With these in mind, a novel donor-π-acceptor (D-π-A) indoline dye, coded as C-RA (Scheme 1), is developed by applying rhodanine-3-acetic acid as the acceptor unit, making it as a panchromatic sensitizer in the true sense. As expected, the absorption of C-RA becomes very broad in visible region, being capable of extending to 800 nm in CH_3CN/CH_2Cl_2 (3/2 v/v). When adsorbed onto 12 μm TiO_2 electrode, its onset wavelength is even extended to about 940 nm in NIR region, showing a preferable overlap with solar light spectrum. However, the plateau IPCE value of C-RA-sensitized DSSCs was only around 10% with an unexpected low power conversion efficiency (0.57–0.90%), one order of magnitude as C-CA (8.49%) under simulated AM 1.5 irradiation. Herein, we are aimed to systematically investigate the distinct difference in photovoltaic performances upon changing the acceptor from cyanoacetic acid (C-CA) to rhodanine-3-acetic acid (C-RA). Considering the preferably broad light-harvesting abilities of C-RA in visible and near-IR region, we carried out the excited electron lifetime measurement and the density functional theory (DFT) calculation to take insight into the poor performance, especially for the relatively low J_{SC}. Meanwhile, the stepped light-induced transient (SLIT) and electrochemical impedance spectroscopy (EIS) measurements were performed on C-CA and C-RA sensitized DSSCs to investigate the charge recombination lifetimes. These studies are highly desirable to the design of novel metal-free organic D-π-A sensitizers, especially for the dyes using rhodanine-3-acetic acid as acceptor.

2. Experimental

2.1. General

The FTO conducting glass (fluorine doped SnO_2, sheet resistance < 15 Ω/square, transmission > 90% in the visible) was obtained from Geao Science and Educational Co. Ltd., China. *tert*-Butylpyridine (TBP) was purchased from Aldrich. Titanium tetrachloride, lithium iodide, 1-butyl-3-methylimidazolium iodide, and deoxycholic acid (DCA) were purchased from Wako Ltd. and used as received. TiO_2 paste (PST-18NR for 20 nm and PST-400C for 400 nm) was provided by JGC C&C Ltd. All other chemicals were produced by Alfa Aesar and used without further purification.

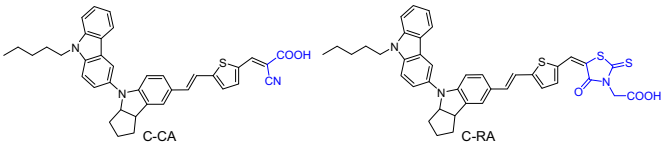

Scheme 1. Chemical structures of C-CA and C-RA with different anchoring groups.

2.2. Characterization

^{1}H NMR and ^{13}C NMR spectra were obtained with a Bruker AV III-500 spectrometer using tetramethylsilane as internal standard. High-resolution mass spectra (HRMS) were recorded on a JEOL LMS-HX-110 spectrometer with 3-nitrobenzyl alcohol (NBA) as a matrix. UV–visible spectra were determined with a Shimadzu UV-2501PC spectrometer. Fluorescent spectra were recorded on Hitachi F-4600 spectrometer. In the measurement of absorption spectra of dye-loaded TiO_2 electrode, the obvious π-aggregation appeared even on the electrode as thin as 4 μm. The aggregation can broaden the absorption spectrum, and cover the absorption peaks. Therefore, in these measurements, 30 mM DCA was added into 0.3 mM dye solution for preventing aggregation. The cyclic voltammograms were measured on a CHI660B electrochemical workstation (CH Instruments) using a normal three-electrodes cell with a dye-loaded TiO_2 electrode as working electrode, a Pt wire auxiliary electrode, and Ag/AgCl reference electrode in saturated KCl solution, 0.1 M tetrabutylammonium hexafluorophosphoric was used as supporting electrolyte. After the measurement, ferrocene was added as the internal reference for calibration.

2.3. Synthesis

C-RA was synthesized according to our previous report except using rhodanine-3-acetic acid instead of cyanoacetic acid [29]. The product was obtained as dark purple solid through column chromatography over silica gel with CH_2Cl_2/CH_3OH mixture (15:1) and recrystallization in CH_2Cl_2/petroleum ether (yield, 47%). ^{1}H NMR (500 MHz, d_6-DMSO, ppm): δ 8.16 (d, J = 7.5 Hz, 1H), 8.10 (s, 1H), 8.00 (s, 1H), 7.69 (d, J = 4.0 Hz, 1H), 7.58–7.62 (m, 2H), 7.41–7.47 (m, 3H), 7.22–7.28 (m, 3H), 7.13–7.19 (m, 2H), 6.61 (d, J = 8.0 Hz, 1H), 5.01 (t, J = 8.5 Hz, 1H), 4.48 (s, 2H), 4.38 (t, J = 6.5 Hz, 2H), 3.86 (t, J = 8.5 Hz, 1H), 2.00–2.11 (m, 1H), 1.61–1.86 (m, 6H), 1.37–1.53 (m, 1H), 1.26–1.35 (m, 4H), 0.83 (t, J = 7.0 Hz, 3H). ^{13}C NMR (125 MHz, d_6-DMSO, ppm): δ 192.2, 166.8, 153.6, 150.6, 141.0, 138.1, 137.3, 135.6, 134.8, 133.9, 133.1, 129.0, 127.2, 126.4, 126.3, 126.1, 123.2, 122.2, 121.8, 121.0, 119.0, 118.3, 116.1, 114.8, 110.4, 109.7, 106.0, 70.2, 47.9, 45.0, 42.8, 35.6, 33.3, 29.2, 28.8, 24.4, 22.4, 14.3. HRMS (TOF MS ES$^+$): m/z calcd for $C_{40}H_{38}N_3O_3S_3$ $[M + H]^+$ 704.2075, found 704.2078.

2.4. Fabrication of solar cells

12 μm Nanocrystalline TiO_2 electrodes with 4 μm scattering layer were prepared and modified following the reported procedure [30]. The thickness of TiO_2 film was measured by a surface profiler (Dektak Co., Ltd., Model DAKTAK II). The dye-loaded electrodes were prepared by dipping TiO_2 electrodes (1.2 cm × 0.8 cm) into 0.3 mM dye solution ($CHCl_3/C_2H_5OH$ = 3/2) with different concentrations of DCA for 5 h. To prepare the counter electrode, the Pt catalyst was deposited on the cleaned FTO glass by coating with a drop of H_2PtCl_6 solution (0.02 M in 2-propanol solution) with the heat treatment at 500 °C for 30 min. In this work, two kinds of electrolytes were used: A) 0.6 M 1-butyl-3-methylimidiazolium iodide (BMII), 0.1 M LiI, 0.05 M I_2 and 0.6 M *tert*-butylpyridine (TBP) in acetonitrile; B) 0.1 M LiI and 0.05 M I_2 in acetonitrile.

2.5. Photovoltaic measurements

Photovoltaic measurements employed an AM 1.5 solar simulator equipped with a 150 W xenon lamp (OTENTO-SUN II, Bunkoukeiki Co., Ltd.). The power of the simulated light was calibrated to 100 mW cm^{-2} using a reference silicon cell (BS-520, Bunkoukeiki Co., Ltd.). *I–V* curves were obtained by applying an external bias to the cell and measuring the generated photocurrent with a Keithley model 2400 digital source meter. The voltage step and delay time of photocurrent were 10 mV and 40 ms, respectively. Cell active area was controlled to be 0.142 cm^2 by a metal mask. The photocurrent action spectra were measured with a monochromator (M10-T, Bunkoukeiki Co., Ltd.). The intensity of monochromic light was calibrated by a reference silicon cell (S1337-1010BQ, Bunkoukeiki Co., Ltd.). Each value in this work was an average of five samples while the standard deviations were lower than ±1%.

Charge recombination lifetime and charge density in the complete DSSCs were measured by the stepped light-induced transient (SLIT) measurements of the photocurrent and voltage based on a DSSCs evaluation system PSL-100 (EKO Co. Ltd.) [31]. A laser (λ = 640 nm) was used as a light source. The transients were induced by a stepwise change in the laser intensity which was controlled by adjusting its voltage. The photocurrent and photovoltage transients were monitored using a digital oscilloscope through an amplifier. Through varying the laser intensity, the lifetime could be estimated over a range of open-circuit voltages by fitting a decay of the photovoltage transient with $\exp(-t/\tau)$ [31]. The charge density measurement was performed in the following method: the DSSCs were illuminated for 5 s while a bias voltage was applied to make the cell to be open-circuited, then the laser was shut down, while simultaneously, the cell was switched from open to short circuit. The resulting current was measured in 25 s, and then the charge density could be calculated through integrating the quantity of electric charge.

Electrochemical impedance spectroscopy (EIS) Nyquist and Bode plot for DSSCs was performed using a two-electrode system under dark. The spectra were scanned in a frequency range of 0.1 Hz to 100 kHz at room temperature with applied bias potential set at −700 mV. The alternate current (AC) amplitude was set at 10 mV. All experiments were conducted at room temperature.

3. Results and discussion

3.1. Photophysical and electrochemical characterization

The photophysical properties of C-CA and C-RA are shown in Fig. 1, and the data are collected in Table 1. The absorption spectrum of C-RA displays two distinct absorption bands in the visible region. The relatively weak band at 392 nm corresponds to the $\pi-\pi^*$ electron transition, while the strong absorption band at 565 nm can be assigned to the intramolecular charge transfer (ICT) between the indoline donor part and the rhodanine-3-acetic acid acceptor part. Compared to C-CA, the change of acceptor group from cyanoacetic acid to rhodanine-3-acetic acid leads to a large bathochromic shift by 42 nm in C-RA, which can be ascribed to the stronger electron withdrawing capability of rhodanine-3-acetic acid than that of cyanoacetic acid. Additionally, the emission peaks of C-CA and C-RA were found at 649 and 817 nm, respectively.

The dye absorption spectra on TiO_2 were further studied with coadsorption of DCA. When loaded on 4 μm TiO_2 electrode (Fig. 1b), dyes C-CA and C-RA exhibited blue-shifted with the value of 32 and 17 nm, respectively. Since the aggregation was prevented by coadsorption of DCA, here the blue-shift of λ_{max} might be predominated by deprotonation effect [25]. When 12 μm TiO_2 electrode was utilized (Fig. 1c), the absorption spectra of two dyes became remarkably broadened. Compared with that on 4 μm TiO_2 electrode, the onset wavelengths of C-CA and C-RA were red-shifted by 67 and 142 nm, respectively. Especially for C-RA, its absorption spectrum can cover an extremely broad region from 370 nm to around 940 nm, along with an absorption plateau from 400 to 700 nm. Here the extended absorption spectrum on thick TiO_2 film was caused by the dye aggregation with higher adsorption

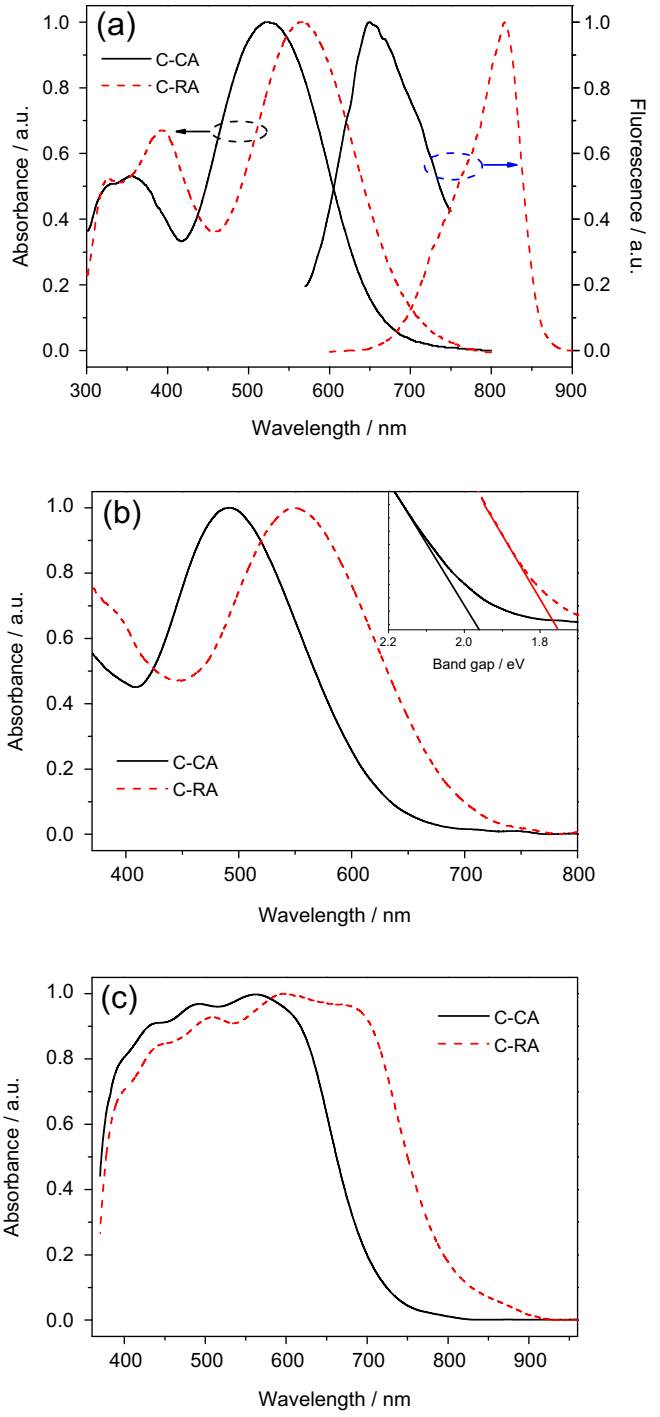

Fig. 1. Normalized absorption and emission spectra of C-CA and C-RA: (a) in CH_3CN/CH_2Cl_2 (3/2 v/v), (b) normalized absorption spectra of the anchored C-CA and C-RA on 4 μm and (c) 12 μm TiO_2 films coadsorbed with 30 mM DCA for preventing aggregation.

Table 1
Absorption and emission properties of C-CA and C-RA.

	λ_{ab}[a]/nm	ε[a]/M^{-1} cm^{-1}	λ_{em}[a]/nm	Stokes shift[b]/nm	λ_{ab}[c]/nm	λ_{onset}[d]/nm
C-CA	523	27,900	649	126	491	850
C-RA	565	18,000	817	252	548	925

[a] Absorption peaks (λ_{ab}), molar extinction coefficient (ε), and emission peaks (λ_{em}) were measured in CH_3CN/CH_2Cl_2 (3/2 in v/v).
[b] Stokes shifts were calculated from λ_{ab} and λ_{em}.
[c] λ_{ab} of the dyes were evaluated on 4 μm TiO_2 electrodes coadsorbed with 30 mM DCA for preventing aggregation.
[d] The onset wavelength (λ_{onset}) of the dyes was obtained on 12 μm TiO_2 electrodes.

amount. Generally, *H*-aggregation makes absorption spectrum blue-shift while *J*-aggregation makes it red-shift. In the case of C-CA and C-RA, although the predominated dye aggregation could be broken on 4 μm TiO_2 film with coadsorption of 30 mM DCA (Fig. 1b), there was still some aggregation when adsorbed onto thicker TiO_2 film (12 μm; Fig. 1c). That is, even the existing of the DCA (30 mM), the *J*-aggregation can take place on the surface of thicker TiO_2 film, which is consistent with previous reports [25,32]. The resulting broad absorption of C-RA is preferably overlapped with solar light spectrum, which is highly beneficial to harvest solar light, even in part of NIR region.

However, the broad absorption spectrum also brings us another problem: the narrow band gap between HOMO and LUMO levels. As shown in Table 2, the band gap ($E_{0\text{-}0}$) of C-RA is only 1.75 V. The narrow band gap can lead the LUMO level more positive, which may have effect on the photo-excited electron injection efficiency. Thus, cyclic voltammograms were performed to evaluate the possibility of electron injection from the excited dye molecules to the conduction band (CB) of TiO_2. C-CA and C-RA show similar HOMO levels as 0.83 and 0.88 V *vs* NHE, respectively. Due to the narrow $E_{0\text{-}0}$, the LUMO level of C-RA is −0.87 V *vs* NHE, more positive than that of C-CA (−1.11 V). As well known, the CB energy level of TiO_2 (E_{CB}) is about −0.5 V *vs* NHE. According to the previous study, a minimal driving force of 0.2 V is sufficient to ensure photo-induced electron injection into the CB of TiO_2 and regeneration of the oxidized dye [33]. Thus, the photo-induced electron injection of both dyes is guaranteed to be efficient in view of thermodynamics.

3.2. Photovoltaic performances

Previously, Uchida et al. have directly attached the acceptor of rhodanine-3-acetic acid with an indoline donor to develop the well-known typical Donor–Acceptor (D–A) featured dyes, such as D102, D149 and D205 [11,17,19]. Impressively, DSSCs based on dye D205 even realized one of records in high power conversion efficiency (9.52%). Once, rhodanine-3-acetic acid was considered as "*amazing*" acceptor for developing metal-free organic sensitizers. Generally, for increasing the light-harvesting and photostability of dyes, the aromatic rings, such as phenyl, fluorenyl, thiophene or oligothiophene segments, are preferable to be utilized [8]. Strangely, when incorporation of rhodanine dye (rhodanine-3-acetic acid) as acceptor into D-π-A configuration with aromatic π-conjugation bridge, the DSSCs based on C-RA exhibited very unexpected low efficiency. Fig. 2 shows the photovoltaic performance of C-CA and C-RA coadsorbed with 30 mM DCA, with IPCE action spectra and *I–V* curves. Disappointedly, although the photoresponsive area of C-RA was extended to about 940 nm, the IPCE values were extremely low. Since the plateau IPCE values were around 10%, the J_{SC} of C-RA was measured to be only 2.83 mA cm^{-2} (Table 3 and Fig. 2).

Table 2
Electrochemical properties of dyes C-CA and C-RA.

	Experimental[a] (V)			Calculated[c] (V)		
	HOMO	$E_{0\text{-}0}$[b]	LUMO	HOMO	$E_{0\text{-}0}$	LUMO
C-CA	0.83	1.94	−1.11	0.41	2.36	−1.95
C-RA	0.88	1.75	−0.87	0.44	2.26	−1.82

[a] Electrochemical properties were measured in CH_3CN using a dye-sensitized TiO_2 electrode as working electrode.
[b] $E_{0\text{-}0}$ values were estimated from the intersection of tangent line and horizontal axis in normalized absorption spectra as shown in Fig. 1b (inset).
[c] Calculated at the B3LYP/6–31G* level in vacuum. Note: the calculated energies were overestimated partially due to the neglect of solvation effect.

Generally, the unbeneficial π-aggregation can quench the excited electrons through intermolecular electron transfer, resulting in a low J_{SC} [4,8]. Hence, different concentrations of DCA as the coadsorbent were applied to inhibit the intermolecular electron transfer process. With increasing the concentration of DCA from 30 to 120 mM, the J_{SC} values were decreased from 2.83 to 1.88 mA cm^{-2}, which might be ascribed to the decrease of dye-loaded amount. Obviously, upon coadsorption with DCA, the intermolecular electron transfer caused by π-aggregation is not the main reason for the low IPCE value.

Firstly, we take account into the low IPCE value of C-RA, which is obviously inconsistent with its broad absorption. As known, the IPCE value is the ratio of the observed photocurrent divided by the incident photon flux (Equation (1)) [34].

$$\mathrm{IPCE} = \mathrm{LHE} \times \Phi_{inj} \times \eta_{el} \quad (1)$$

where LHE is the light harvesting efficiency, Φ_{inj} is the excited electron injection yield, and η_{el} is the electron collection efficiency. Since closely related to the structural morphology of TiO_2 layer,

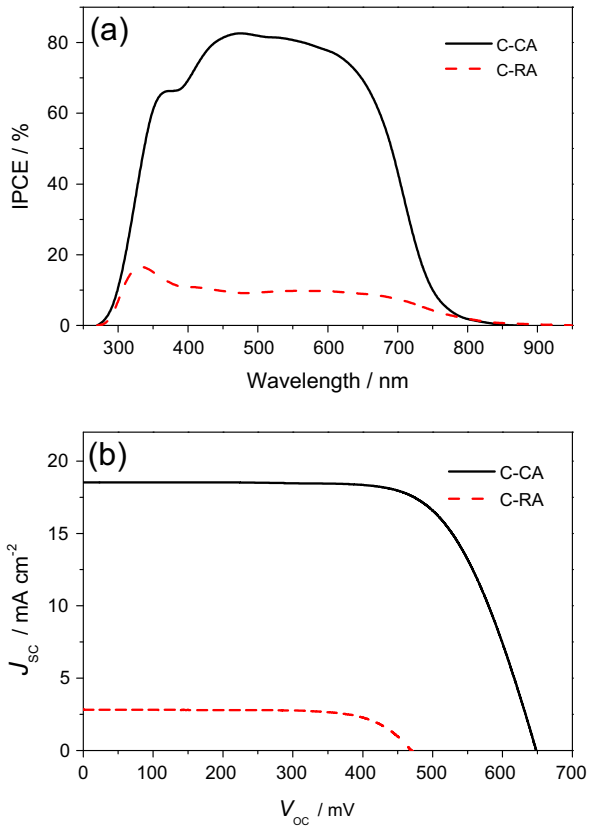

Fig. 2. (a) IPCE action spectra and (b) *I–V* curves of C-CA and C-RA sensitized DSSCs with 30 mM DCA as co-adsorbed materials.

Table 3
Current–voltage characteristics for DSSCs based on C-CA and C-RA with different concentrations of DCA and electrolytes.

	Electrolyte	DCA (mM)	J_{SC} (mA cm^{-2})	V_{OC} (mV)	*ff*	η (%)
C-CA	A	30	18.53	649	0.71	8.49
C-RA	A	30	2.83	472	0.68	0.90
	A	60	2.73	475	0.69	0.87
	A	90	2.57	471	0.69	0.83
	A	120	1.88	462	0.67	0.57
	B	30	2.92	389	0.62	0.68

here η_{el} for two dyes should be similar due to the same preparation conditions of TiO_2 electrodes. Accordingly, the possible reason for the low IPCE value in C-RA is correlated with the low LHE or Φ_{inj}.

LHE value is dependent upon the photophysical properties of sensitizers. As shown in Fig. 3, LHE spectra of two dyes are calculated from the absorption spectra of dye-loaded 12 μm TiO_2 electrodes. C-RA shows an extremely broad light harvesting area from 370 to 940 nm, including a plateau of 400–730 nm with high value (>90%). Obviously, C-RA possesses much better LHE performance than that of C-CA. As a consequence, the distinctly difference of IPCE values between C-CA and C-RA can be predominately attributed to the excited electron injection yield (Φ_{inj}), which critically depends on the excited electron lifetime and redox potentials of dyes [4].

As discussed above, the LUMO level of C-RA was calculated to be −0.87 V, which is negative enough to ensure electron injection from the excited states into the conduction band of TiO_2 (E_{CB} −0.5 V). However, the E_{CB} will up-shift in the presence of some additives in the electrolyte, such as *tert*-butylpyridine (TBP) or *N*-methylbenzimidazole (BMII) [35]. Thus, we removed TBP and BMII from the I/I_3 electrolyte, that is, using electrolyte B to fabricate DSSCs to see whether there was an obvious increase in J_{SC} or not. The *I–V* data are also listed in Table 3. When the additives were removed from the electrolyte, the J_{SC} value was only increased by less than 5%. Therefore, even in the presence of TBP and BMII additives in the electrolyte (electrolyte A), there is enough driving force for the photo-induced electron injection from the LUMO level of C-RA to the E_{CB} of TiO_2. Therefore, considering the compatible redox potential as well as broad LHE, the observed extremely low IPCE and J_{SC} for C-RA can be definitely attributed to the low electron injection yield (Φ_{inj}) with short electron lifetime.

Next, we focus on the difference in the excited electron lifetime of dyes C-CA and C-RA. As listed in Table 1, an extraordinary large Stokes shift was obtained for C-RA (252 nm), which was twice as long as that of C-CA (126 nm). That means, upon light irradiation, the excited electrons of C-RA are easier to release energy through the decay process than that of C-CA, suggesting that C-RA may have relatively short excited electron lifetime. Generally, in DSSCs, it takes more than a hundred picoseconds to finish the excited electron injection process [36]. Accordingly, there exists a serious competition between the electron injection and non-radiative decay when the excited electron lifetime is too short (even at picosecond level). The excited electron lifetimes of C-RA and C-CA loaded TiO_2 films were measured, respectively. As expected, the excited electron lifetime of C-RA on TiO_2 film was only about 480 ps, almost at the same level with the electron injection process. In contrast, the relative electron lifetime of C-CA was measured to be 2.54 ns, which was 5.2 fold as that of C-RA. Obviously, compared with C-CA, the short excited electron lifetime in C-RA causes the serious competition between the electron injection and non-radiative decay, leading to low electron injection efficiency.

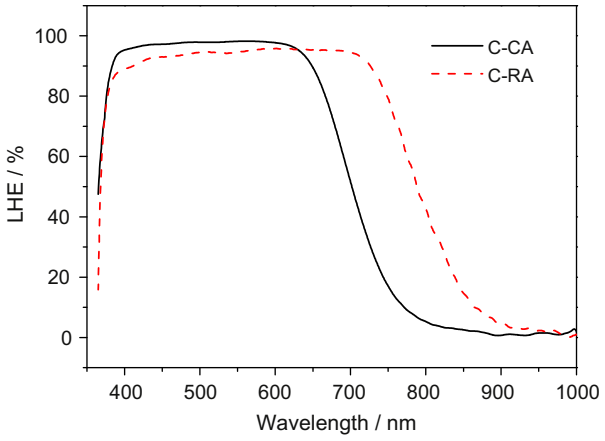

Fig. 3. LHE spectra of C-CA and C-RA calculated from the absorption spectra of dye-loaded 12 μm TiO_2 electrodes.

3.3. DFT simulation

To get further insight into the distinct difference in the photovoltaic performances of C-CA and C-RA, DFT calculation was carried out on a B3LYP/6–31 + G(d) level for the geometry optimization [37]. As shown in Fig. 4, the HOMO orbital of C-CA is delocalized throughout the whole structure, and the LUMO orbital mainly locates at the linker and extends through the anchoring units. In contrast, the LUMO electrons of C-RA are isolated from the carboxyl anchoring group (−CH_2CO_2H) due to the presence of the methylene group, which may suppress the electron injection efficiency from the excited dyes to the CB of TiO_2. Therefore, the electron destiny of LUMO for C-RA does not closely overlap with the conduction of TiO_2, potentially resulting in the predominance toward injecting electrons closer to the TiO_2 surface with low electron injection efficiency (Fig. 5).

From the DFT analysis, here we consider that the methylene group between the rhodanine and carboxylic acid may severely disrupt the electronic coupling of dye and TiO_2, thus lowering the efficiency of photo-excited electron injection. Obviously, it seems conflict with the high efficiency photovoltaic dyes, such as D102, D149 and D204 [11,17,19], which also contains a similar anchoring group as that of the C-RA. Indeed, these D-series dyes have well demonstrated with high photovoltaic efficiency. However, the chemical structures of D102, D149, and D205 are quite different from the sensitizer C-RA, with the following considerations:

(i) *The different dye configuration between D-series dyes and C-RA.* In D102, D149, and D205 sensitizers, the donor (indoline part) and acceptor (rhodanine part) are connected directly without any aromatic π-linker, that is, these D-series dyes belong to typical D–A type sensitizers. Thus, the LUMO orbital of these sensitizers is mainly distributed on rhodanine part, affording much higher possibilities for electron injection. However, C-RA belongs to a typical D-π-A feature (Scheme 1). Upon incorporation of an additional thiophene unit as conjugation bridge, the electron distribution of LUMO orbital in C-RA is mainly delocalized over both π-linker segment bridge and rhodanine framework. With respect to the counterpart C-CA containing cyanoacetic acid, the electron destiny on the anchoring group of CO_2H is negligible in the system of C-RA containing rhodanine-3-acetic acid.

(ii) *In the two rhodanine units combining together as the acceptor, the anchoring interaction with TiO_2 might become very complicated.* In the D–A system of D102 containing a single rhodanine unit, the photovoltaic efficiency is lower than D149 and

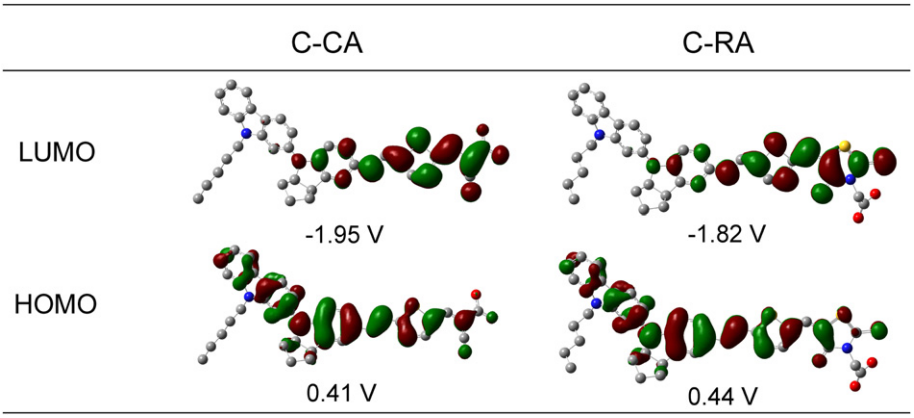

Fig. 4. Calculated frontier orbitals of compounds C-CA and C-RA (isodensity = 0.020 a.u.).

D205. Moreover, in chemical structures of D149 and D205, the acceptor unit contains additional rhodanine unit, that is, two rhodanine units combine together as the acceptor, which will enhance the electron-withdrawing capability of acceptor and further move the electron density distribution of LUMO orbital to rhodanine-3-acetic acid unit. Specifically, in the two-rhodanine units as acceptor, the anchoring interaction with TiO_2 might become very complicated, not limited to the carboxylic group. The two carbonyl groups in the each rhodanine can also play much role on guaranteeing the efficient electron injection. Recently, Tian et al. have reported a nice work on the modified rhodanine acceptor [38]. In the modified acceptor of 2-(1,1-dicyanomethylene)rhodanine, the formation of coordinate bonds between the O and N in the middle acceptor rhodanine of RD-I and RD-II tautomers and the Lewis acid sites of the TiO_2 surface guarantee efficient electron injection from the dyes to TiO_2.

Therefore, the mono- or double-rhodanine unit as acceptor is sensitive to the dye configuration and the anchoring interaction. Overall, the low photo-excited electron injection yield results in the low photovoltaic performance of C-RA, which does not conflict with the high photovoltaic performance of D-series sensitizers. With the investigation of excited electron lifetime discussed above, the back-electron-transfer between the photo-excited electrons and the oxidized sensitizer is prone to take place, resulting in relatively low electron injection efficiency with low J_{SC} [3,4].

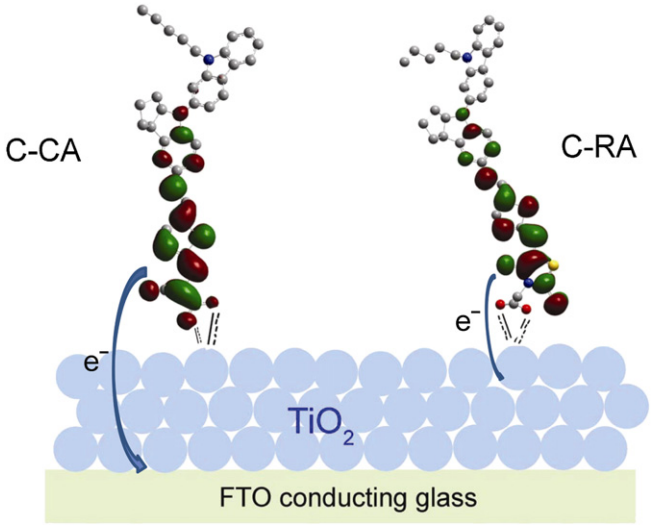

Fig. 5. Schematic electron injection process of C-CA and C-RA.

3.4. Charge recombination

Besides the low J_{SC}, the V_{OC} of C-RA was also lower than that of C-CA by about 177 mV, and obtained as 472 mV. To further investigate the internal reason for the low photovoltage, the V_{OC} and charge recombination lifetime as a function of charge density based

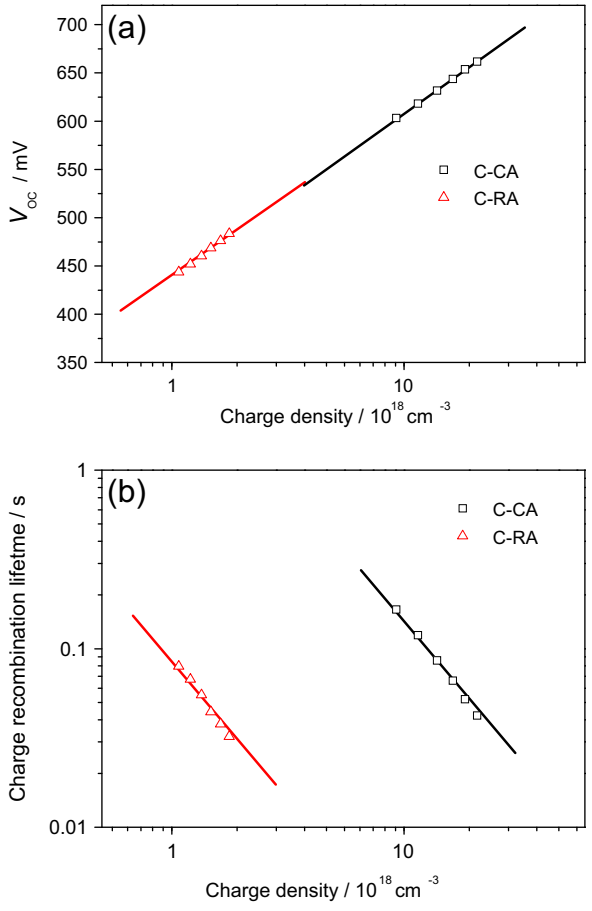

Fig. 6. (a) Open-circuit voltage (V_{OC}) and (b) charge recombination lifetime as a function of charge density based on C-CA and C-RA-sensitized solar cells.

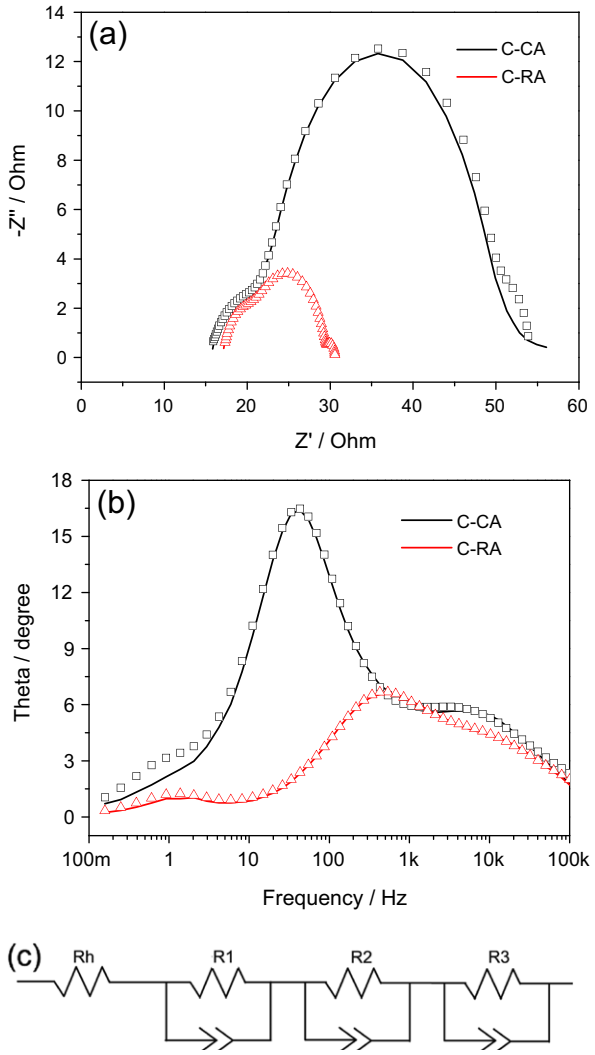

Fig. 7. EIS Nyquist (a), Bode (b) plots and equivalent circuit (c) for DSSCs based on C-CA and C-RA measured in the dark. The scatters of (a) and (b) show theoretical fits using the equivalent circuit.

on C-CA and C-RA sensitized DSSCs in the presence of DCA were measured by the SLIT measurements. Generally, the V_{OC} is determined by the difference between the quasi-Fermi level of TiO_2 (E_{Fn}) and the potential of the redox couple (E_{redox}, I^-/I_3^- in this work) in electrolyte. The quasi-Fermi level is associated with both the E_{CB} and the charge density in TiO_2 (Equation (2)) [39]:

$$E_{Fn} = E_{CB} + kT \ln(n/N_c) \quad (2)$$

where n is the injection charge density in the TiO_2 electrode and N_c is the effective density of states in the CB, and the ratio n/N_c is determined by the balance between electron injection and charge recombination. Generally, n/N_c value becomes higher when the electron injection is more effective, resulting in longer charge recombination lifetime. From Equation (2), both increasing charge density in TiO_2 and decreasing the charge recombination rate can move E_{Fn} to be more negative and give higher V_{OC}.

In Fig. 6a, when illuminating cell devices with the same light intensity, the electron densities of C-CA and C-RA were measured to be 20.65×10^{18} and 1.77×10^{18} cm^{-3}, respectively. Thus, in Equation (2), the n value of C-RA was less than one tenth of that of C-CA, in consistent with the poor Φ_{inj} value as discussed above in LHE analysis. Also, two curves of DSSCs based on C-CA and C-RA exhibited the similar slope, which were almost coincided with each other. At a given charge density in the SLIT measurements, here the almost same V_{OC} for the two dyes based DSSCs indicates the identical E_{CB} for two cases. That is, the E_{CB} is not influenced so much by changing the acceptor units from cyanoacetic acid to rhodanine-3-acetic acid.

Because there is no obvious change in the CB of TiO_2 (E_{CB}) sensitized with the two dyes, the significant difference in photovoltage of DSSCs should be attributed to the different charge recombination rate. As shown in Fig. 6b, the charge recombination lifetime decreases with charge density, and follows a power law relation with the same slope, indicative of the same recombination mechanism [26]. Obviously, the charge recombination lifetimes for DSSC based on C-CA are much longer than that of C-RA at a given charge density.

To complement the SLIT measurements, electrochemical impedance spectroscopy (EIS) measurements were also conducted to investigate the charge recombination lifetimes directly in these devices. Fig. 7 shows the Nyquist and Bode plots for C-CA and C-RA sensitized DSSCs measured under dark. In the Nyquist diagram, three semicircles from left to right are visible, and represent the impedances of the charge transfer on the Pt counter electrode (R_1, smaller circles), the charge recombination at TiO_2/dye/electrolyte interface (R_2, larger circles), and carrier transport within electrolyte (R_3, smaller circles on the right). As listed in Table 4, two dyes show similar R_h and R_1 values due to the same electrolyte and electrode in both materials and surface area. The charge recombination impedance of C-RA (R_2), corresponding to the diameter of middle frequency semicircle of Nyquist plot, was calculated to be 8.9 Ohm cm^{-2}, which was less than one third of that of C-CA (27.5 Ohm cm^{-2}). Here a smaller R_2 value means faster charge recombination rate between the CB of TiO_2 and the electrolyte, indicating that the charge recombination lifetime of C-RA is shorter than that of C-CA.

To determine the charge recombination lifetime directly, the reaction resistance of DSSCs was analyzed by ZSimpWin using an equivalent circuit shown in Fig. 7c. The charge recombination lifetime can be calculated through Equation (3).

$$\tau_e = 1/(2\pi f) \quad (3)$$

where f is the peak frequency in EIS Bode plot. For C-RA, the charge recombination lifetime was calculated to be 296 μs, which is only

Table 4
Parameters obtained by fitting the impedance spectra using the equivalent circuit.[a]

	R_h[b]/Ohm cm^{-2}	CPE_1[c]/μF cm^{-2}	n_1[d]	R_1[b]/Ohm cm^{-2}	CPE_2[c]/μF cm^{-2}	n_2[d]	R_2[b]/Ohm cm^{-2}	CPE_3[c]/μF cm^{-2}	n_3[d]	R_3[b]/Ohm cm^{-2}
C-CA	15.4	293.5	0.80	7.7	283.4	0.80	27.5	51,870	0.8	3.5
C-RA	17.1	31.6	0.82	3.7	240.0	0.79	8.9	0.1113	1.0	0.9

[a] Equivalent circuit of the DSSC consisting of TiO_2/dye/electrolyte and Pt/electrolyte interface.
[b] R_h, R_1, R_2, R_3 are the series resistance of Pt and TCO, charge-transfer resistance at Pt/electrolyte, at TiO_2/dye/electrolyte interface, and carrier transport within electrolyte, respectively.
[c] CPE_1, CPE_2, and CPE_3 are the constant phase element for the TiO_2/dye/electrolyte, Pt/electrolyte interface, and carrier transport within electrolyte, respectively.
[d] n presents the degree of surface inhomogeneity.

about one thirteenth of that of C-CA (3902 μs). Therefore, the trends of charge recombination lifetime observed from SLIT and EIS measurements are identical. As an overall result of lower charge density and shorter charge recombination lifetime, C-RA presented much lower V_{OC} of 472 mV than that of C-CA (649 mV). We note that in EIS measurements, DCA was not added as the co-adsorbed material, thus the charge recombination lifetime of both dyes were relatively short. However, it will not affect the trend discussed here.

4. Conclusion

We developed a novel D-π-A organic dye C-RA by incorporating a carbazole substituted indoline as donor group and rhodanine-3-acetic acid as anchoring group to enhance light-harvesting ability. By replacement of cyanoacetic acid with rhodanine-3-acetic acid, the onset wavelength of photoresponsive area for dye C-RA is red-shifted to 940 nm with high LHE values. However, the plateau IPCE value of C-RA sensitized DSSCs was only around 10%, resulting in an extremely low photovoltaic performance (J_{SC} 2.83 mA cm^{-2}, V_{OC} 472 mV, *ff* 0.68, and η 0.90%). The power conversion efficiency of DSSCs based on C-RA (0.57–0.90%) is one order of magnitude with respect to C-CA (8.49%). With the systematic studies on LHE, SLIT and EIS measurements as well as DFT analysis, our results reveal that the poor photovoltaic performance for C-RA is attributed to the following possible characteristics arising from the rhodanine segment: i) the relatively short excited electron lifetime and the isolation of LUMO orbital from anchoring group, resulting in the low photo-excited electron injection efficiency with low J_{SC}; ii) an overall result of the low injection charge density in the TiO_2 electrode and fast charge recombination rate leading to the low V_{OC}. The analysis of EIS Bode plot indicates that the charge recombination lifetime for C-RA is about 296 μs, which is only about one thirteenth of that of C-CA (3902 μs). Moreover, the mono- or double-rhodanine unit as acceptor is sensitive to the dye configuration and the anchoring interaction, which does not conflict with the high photovoltaic performance of D-series sensitizers. With respect to dyes D102, D149 and D205, the low photo-excited electron injection yield and the fast charge recombination rate results in the observed extremely low photovoltaic performance of C-RA. These findings will afford powerful strategy for future development of efficient organic sensitizers, especially for those using rhodanine-3-acetic acid as acceptor unit in D-π-A configuration.

Acknowledgments

This work was supported by National Natural Science Foundation of China (21102034 and 21176075), the Science Foundation for the Excellent Youth Scholars of Hebei Province (Y2012017), the Nature Science Foundation of Hebei Province (B2012205001) Grant-in-Aids for Scientific Research (A) (23245036, YN), National 973 Program (2013CB733700), the Oriental Scholarship, the Fundamental Research Funds for the Central Universities (WK1013002), and the Open Funding Project of State Key Laboratory of Luminescent Materials and Devices (SCUT).

References

[1] B. O'Regan, M. Grätzel, Nature 353 (1991) 737.
[2] J. Roncali, Adv. Energy Mater. 1 (2011) 147.
[3] J. Wiberg, T. Marinado, D.P. Hagberg, L.C. Sun, A. Hagfeldt, B. Albinsson, J. Phys. Chem. C 113 (2009) 3881.
[4] Z.J. Ning, Y. Fu, H. Tian, Energy Environ. Sci. 3 (2010) 1170.
[5] J. Yoon, D.K. Kang, J. Won, J.Y. Park, Y.S. Kang, J. Power Sources 201 (2012) 395.
[6] A. Mishra, M.K.R. Fischer, P. Bäuerle, Angew. Chem. Int. Ed. 48 (2009) 2474.
[7] M.K.R. Fischer, S. Wenger, M.K. Wang, A. Mishra, S.M. Zakeeruddin, M. Grätzel, P. Bäuerle, Chem. Mater. 22 (2010) 1836.
[8] A. Hagfeldt, G. Boschloo, L. Sun, L. Kloo, H. Pettersson, Chem. Rev. 110 (2010) 6595.
[9] J.A. Mikroyannidis, D.V. Tsagkournos, P. Balraju, G.D. Sharma, J. Power Sources 196 (2011) 4152.
[10] J. Zhang, H.-B. Li, S.-L. Sun, Y. Geng, Y. Wu, Z.-M. Su, J. Mater. Chem. 22 (2012) 568.
[11] T. Horiuchi, H. Miura, S. Uchida, Chem. Commun. (2003) 3036.
[12] T. Horiuchi, H. Miura, S. Uchida, J. Photochem. Photobiol. A 164 (2004) 29.
[13] Md. K. Nazeeruddin, A. Kay, I. Rodicio, R. Humphry-Baker, E. Mueller, P. Liska, N. Vlachopoulos, M. Grätzel, J. Am. Chem. Soc. 115 (1993) 6382.
[14] J.H. Yum, I. Jung, C. Baik, J. Ko, M.K. Nazeeruddin, M. Grätzel, Energy Environ. Sci. 2 (2009) 100.
[15] Y. Chiba, A. Islam, Y. Watanabe, R. Komiya, N. Koide, L.Y. Han, Jpn. J. Appl. Phys. Part 2 45 (2006) L638.
[16] Md. K. Nazeeruddin, P. Pechy, M. Grätzel, Chem. Commun. (1997) 1705.
[17] T. Horiuchi, H. Miura, K. Sumioka, S. Uchida, J. Am. Chem. Soc. 126 (2004) 12218.
[18] S. Ito, S.M. Zakeeruddin, R. Humphry-Baker, P. Liska, R. Charvet, P. Comte, Md. K. Nazeeruddin, P. Péchy, M. Takata, H. Miura, S. Uchida, M. Grätzel, Adv. Mater. 18 (2006) 1202.
[19] S. Ito, H. Miura, S. Uchida, M. Takata, K. Sumioka, P. Liska, P. Comte, P. Péchy, M. Grätzel, Chem. Commun. (2008) 5194.
[20] M. Akhtaruzzaman, A. Islam, F. Yang, N. Asao, E. Kwon, S.P. Singh, L. Han, Y. Yamamoto, Chem. Commun. 47 (2011) 12400.
[21] S. Higashijima, H. Miura, T. Fujita, Y. Kubota, K. Funabiki, T. Yoshida, M. Matsui, Tetrahedron 67 (2011) 6289.
[22] K. Premaratne, G.R.A. Kumara, R.M.G. Rajapakse, M.L. Karunarathne, J. Photochem. Photobiol. A 229 (2012) 29.
[23] B. Liu, W. Zhu, Q. Zhang, M. Xu, Z. Ning, Y. Xie, H. Tian, Chem. Commun. (2009) 1766.
[24] B. Liu, W. Wu, X. Li, L. Li, S. Guo, X. Wei, W. Zhu, Q. Liu, Phys. Chem. Chem. Phys. 13 (2011) 8985.
[25] W. Zhu, Y. Wu, S. Wang, W. Li, X. Li, J. Chen, Z.-S. Wang, H. Tian, Adv. Funct. Mater. 21 (2011) 756.
[26] Y. Cui, Y. Wu, X. Lu, X. Zhang, G. Zhou, F. Miapeh, W. Zhu, Z.-S. Wang, Chem. Mater. 23 (2011) 4394.
[27] Y. Wu, X. Zhang, W. Li, Z.-S. Wang, H. Tian, W. Zhu, Adv. Energy Mater. 2 (2012) 149.
[28] W. Li, Y. Wu, Q. Zhang, H. Tian, W. Zhu, ACS Appl. Mater. Interf. 4 (2012) 1822.
[29] B. Liu, Q. Liu, D. You, X. Li, Y. Naruta, W. Zhu, J. Mater. Chem. 22 (2012) 13348.
[30] S. Ito, T.N. Murakami, P. Comte, P. Liska, C. Grätzel, Md. K. Nazeeruddin, M. Grätzel, Thin Solid Films 516 (2008) 4613.
[31] S. Nakade, T. Kanzaki, Y. Wada, S. Yanagida, Langmuir 21 (2005) 10803.
[32] A. Mishra, R.K. Behera, P.K. Behera, B.K. Mishra, G.B. Behera, Chem. Rev. 100 (2000) 1973.
[33] (a) G. Boschloo, A. Hagfeldt, Acc. Chem. Res. 42 (2009) 1819;
(b) S. Wenger, P.A. Bouit, Q. Chen, J. Teuscher, D.D. Censo, R. Humphry-Baker, J.E. Moser, J.L. Delgado, N. Martín, S.M. Zakeeruddin, M. Grätzel, J. Am. Chem. Soc. 132 (2010) 5164.
[34] K. Kalyanasundaram, M. Grätzel, Coordin. Chem. Rev. 177 (1998) 347.
[35] T. Stergiopoulos, P. Falaras, Adv. Energy Mater. 2 (2012) 616.
[36] A. Listorti, B. O'Regan, J.R. Durrant, Chem. Mater. 23 (2011) 3381.
[37] M.J. Frisch, G.W. Trucks, H.B. Schlegel, P.M.W. Gill, B.G. Johnson, M.A. Robb, J.R. Cheeseman, T. Keith, G.A. Petersson, J.A. Montgomery, K. Raghavachari, M.A. Al-Laham, V.G. Zakrzewski, J.V. Ortiz, J.B. Foresman, J. Cioslowski, B.B. Stefanov, A. Nanayakkara, M. Challacombe, C.Y. Peng, P.Y. Ayala, W. Chen, M.W. Wong, J.L. Andres, E.S. Replogle, R. Gomperts, R.L. Martin, D.J. Fox, J.S. Binkley, D.J. Defrees, J. Baker, J.P. Stewart, M. Head-Gordon, C. Gonzalez, J.A. Pople, Gaussian 03, Revision E.01, Gaussian, Inc., Pittsburgh, PA, 2004.
[38] J.Y. Mao, N.N. He, Z.J. Ning, Q. Zhang, F.L. Guo, L. Chen, W.J. Wu, J.L. Hua, H. Tian, Angew. Chem. Int. Ed. 51 (2012) 9873.
[39] F. Fabregat-Santiago, G. Garcia-Belmonte, I. Mora-Séro, J. Bisquert, Phys. Chem. Chem. Phys. 13 (2011) 9083.